Investigation of the Ffowcs-Williams and Hawkings Analogy on an Isolated Landing Gear Wheel

Antoine Hajczak, Laurent Sanders, Vuillot François, Philippe Druault

Investigation of the Ffowcs-Williams and Hawkings Analogy on an Isolated Landing Gear Wheel

Antoine Hajczak*, Laurent Sanders †, François Vuillot ‡
ONERA - The French Aerospace Lab, F-92322 Châtillon, France

Philippe Druault§
Sorbonne Université UPMC Paris 6, CNRS UMR 7190,
Institut Jean le Rond d'Alembert, F-75005 Paris, France

This paper addresses the use of the so-called solid and permeable formulations of the Ffowcs-Williams & Hawkings (FW-H) equation in the scope of bluff body noise predictions. The aerodynamic turbulent flow is computed around and downstream of an isolated landing gear wheel from the LAGOON configuration by means of a Zonal Detached Eddy Simulation initiated in a previous study at a Mach number of 0.23. The aerodynamic field obtained with this simulation is then used to compute the FW-H integral respectively on the wheel solid walls and on a permeable surface that encloses the wheel and the most turbulent portion of its wake. The solid FW-H results are shown to be little influenced by the accurate resolution of the wake, with differences in the integrated levels of less than 2 dB only in the upstream direction. The comparison between the solid and permeable formulation results allows to check that at this Mach number, the quadrupolar contribution of the sources present in the wake of this landing gear wheel can be discarded for Strouhal numbers up to 19.3 (5 kHz). As previously observed in several studies, removing the endcap closure of the permeable surface reduces the spurious noise induced by the eddies passing through it. The influence of the FW-H surface discretisation is assessed by considering two levels of resolution. In this study, refining the outflow surface has shown to greatly reduce the spurious noise while the integration surface was kept closed.

I. Nomenclature

PSD	=	Power Spectral Density	ϕ	=	Azimuthal angle
FW-H	=	Ffowcs-Williams & Hawkings	θ	=	Polar angle
RANS	=	Reynolds-Averaged Navier-Stokes	f	=	Frequency
Z-DES	=	Zonal Detached Eddy Simulation	St_{D_w}	=	Strouhal number based on the wheel diameter = $\frac{fD_w}{U_\infty}$
OASPL	=	Overall Sound Pressure Level	Σ	=	FW-H integration surface
D_w	=	Wheel diameter	$\vec{n}$	=	Outward unit normal vector
h	=	Cavity depth	$\vec{v}^{\Sigma}$	=	FW-H surface velocity vector
r	=	Wheel cavity radius	H	=	Heavyside function
κ	=	Cavity depth to diameter ratio = $\frac{h}{2r}$	δ	=	Dirac function
P	=	Pressure	T_{ij}	=	Lighthill stress tensor
T	=	Temperature	δ_{ij}	=	Kronecker symbol
ρ	=	Density	dS	=	Surface element
x, y, z	=	Cartesian components	c	=	Sound speed
u, v, w	=	Cartesian velocity components	Δ	=	Local cell diameter
M	=	Mach number	$M1, M2$	=	Mesh 1, Mesh 2
Δt	=	Time-step	U_∞	=	Upstream flow velocity
T_{D_w}	=	Wheel diameter based convective time = $\frac{D_w}{U_\infty}$			

*PhD student, DAAA - Dept. of Aerodynamics, Aeroelasticity and Acoustics, antoine.hajczak@onera.fr
†Research scientist, DAAA - Dept. of Aerodynamics, Aeroelasticity and Acoustics, laurent.sanders@onera.fr
‡Scientific advisor, DMPE - Dept. of Multi-Physics for Energetics, francois.vuillot@onera.fr, AIAA senior member
§Associate professor, Institut Jean le Rond d'Alembert, philippe.druault@upmc.fr

II. Introduction

The aeronautical industry is currently facing the challenge of managing its environmental impact in order to accommodate the continued growth of both civilian air traffic and suburban areas. More and more people, as well as ecosystems, are being subject to noise pollution, and its mitigation has consequently become a major issue. Within the last decades, jet noise has been extensively addressed by the aeroacoustic community, leading to the design of much quieter turbofan engines. This reduction in engine noise has given way to other noise sources that were of secondary concern before, particularly at landing conditions, when aircraft noise is the most importunate. Indeed, the unsteady turbulent flow around high-lift devices and especially landing gears has proven to generate noise levels that could reach the ones related to the engines when operating at reduced thrust. The predominance of landing gear among airframe noise can be explained by its extremely complicated geometry that comprises a large number of blunt bodies of various size and shape. This particularity has two major consequences. First, complex aeroacoustic mechanisms take place due to massive flow detachments and multiple interactions of turbulent wakes with solid surfaces. Second, the computation of the turbulent flow in the vicinity of the gear can be challenging because of the grid work required, especially if a structured approach is adopted. At first, noise predictions of landing gears relied on the use of semi-empirical models (eg Fink [1] and Guo [2]) but over the last decades, the progress achieved in computational fluid dynamics as well as the increase in computational power has allowed the simulation of the turbulent flow field around a landing gear of moderate complexity with very good accurracy [3–6]. In aeroacoustic studies, the quantity of interest is the far-field acoustic pressure radiated by the interaction of the landing gear with the flow. However, its direct computation still remains unaffordable and noise predictions of a particular landing gear geometry rely most of the time on hybrid methods. These methods consist in two steps that are (i) the computation of the unsteady turbulent flow in the vicinity of the gear thanks to a Navier-Stokes or Lattice-Boltzmann Method solver and (ii) the extrapolation of the turbulent flow to far-field acoustic perturbations by means of an acoustic analogy. Since the seminal work of Lighthill, several acoustic analogies have been derived. The most popular in the case of landing gear noise is the Ffowcs-Williams & Hawkings [7] (FW-H) analogy that consists in an inhomogeneous wave equation with source terms accounting for the presence of solid surfaces. The resolution of this equation leads to the integration of the source terms on an arbitrary closed control surface and in its outer volume. The interpretation of the FW-H equation can further lead to two formulations known respectively as the *permeable* and *solid* formulations, depending on how the integration surface is chosen. The most general is the permeable one and is very similar to the Kirchhoff method. This formulation takes into account the quadrupolar volume sources enclosed by the integration surface as well as the interaction with the solid surface of the body. Despite its general nature, this formulation has the main drawback of being computationally expensive (memory and CPU) and leads to problems related to the crossing of the surface by the wake of the body. This issue is well known and has been observed in many studies. Among others, Mendez et al. [8] have established a "best practices" list in order to cope with the problems that can arise with the use of the permeable surface. The second formulation is the solid one and is the most popular in landing gear noise predictions as it avoids the problems related to the wake and is additionally less computationally expensive. These advantages come with the major hypothesis that the quadrupolar sound in the wake of the body is negligible. A specificity of landing gear noise is that, by definition, it is only relevant in landing phase where the Mach number upper bound for a commercial airplane is roughly 0.25. This argument is often invoked to justify the use of the solid formulation as it is commonly stated that, at low Mach number, the dipolar sound is much more efficient than the quadrupolar sound as their contributions scale respectively with M^6 and M^8. This result, however, has been questioned, by Spalart [9] who found that the scaling law for quadrupoles *in the presence of dipoles* was M^7, rather than M^8.

Furthermore, the use of a formulation instead of the other remains controversial in the scope of bluff body noise predictions as some studies have led to interesting results with the permeable one. For example, Spalart et al. [6] and Souliez et al. [10] have found a possible importance of near-field quadrupoles with the permeable surface for Mach numbers below 0.23. Additionally, Greschner at al. [11] have even pointed out that the quadrupolar sound emitted by a rod airfoil configuration at M=0.2 was no longer negligible and that the permeable formulation better matched the experimental results of Jacob et al. [12] at high frequencies for an integration surface surrounding the whole rod-airfoil system and a portion of its wake.

Among the components of a landing gear, wheels are a major contribution to the acoustic far-field radiation [13] and have gained considerable attention over the past few years [14–18]. Moreover, the wheels of a landing gear contribute significantly to the turbulent wake of the whole gear, hence potentially inducing noise sources of quadrupolar nature. This is even more plausible in the case of a four-wheel landing gear, as the wheel-to-wheel interaction generates an intense turbulent wake.

The aim of this paper is to assess the use of the FW-H equation in the scope of landing gear noise predictions at low Mach number. In particular, this paper aims at clarifying (i) the influence of the wake resolution on the solid FW-H results, (ii) the role of the quadrupole noise in the case of an isolated wheel and (iii) the effects related to the problem of the outflow surface when the permeable surface approach is chosen.

It is organised in two sections. The first one is dedicated to the description of the test case and aerodynamic results. The second one presents the results of the FW-H computations and their interpretation.

III. Description of the test case and flow features

This paper further investigates the noise emitted by an isolated landing gear wheel from the LAGOON geometry initiated in a previous paper [17]. In this section, the wheel geometry and main dimensions are first briefly recalled. Then, the numerical setup for the computation of the turbulent flow as well as the FW-H surface integral are described. Finally, an analysis of the wake downstream of the wheel is carried out in order to quantify the passage of the wake across the FW-H surface, which is known to be a critical issue in noise predictions.

A. Geometry and computational setup

1. Main dimensions of the LAGOON wheel

The LAGOON geometry (see figure 1a) is a 1:2.5 scaled canonical two-wheel nose landing gear which has been designed in the scope of the LAGOON experimental campaign led by Manoha et al. [19, 20] in 2007. This campaign then brought together several teams to compare their numerical computations to the experimental results in the framework of the Benchmark on Airframe Noise Computation (BANC). These computations included structured and unstructured methods, Chimera techniques, and Lattice-Boltzmann Methods (for a detailed review of these contributions, please refer to the summary presented by Manoha et al. [21] in 2015).

A single wheel from this geometry, without the axle, will be considered in this study (see figure 1b). Its external diameter is $D_w = 0.3m$ and the whole wheel can basically be considered as an installed shallow round cavity of internal radius $r = 0.081m$ and depth $h = 0.037m$. Cavity noise is a phenomenon that has been extensively covered by the aeroacoustic community. Hence, cavities are classified according to their depth to diameter ratio κ. In the case of the LAGOON cavity, this parameter has a value $\kappa = 0.23$, which ranks it in the shallow cavities category.

A common feature of cavity flows is that they often induce a strong tonal response that is attributed by several authors to the coupling between a depth mode and a Rossiter-like feedback loop [22, 23]. Casalino et al. [14] have studied the two facing wheels of the LAGOON geometry and numerically recovered the tonal peaks at 1 and 1.5kHz already observed in the LAGOON experiments [19]. Previous work on the isolated wheel showed that the 1.5kHz tone was still present, but much weaker than in the case of the two facing wheels [17].

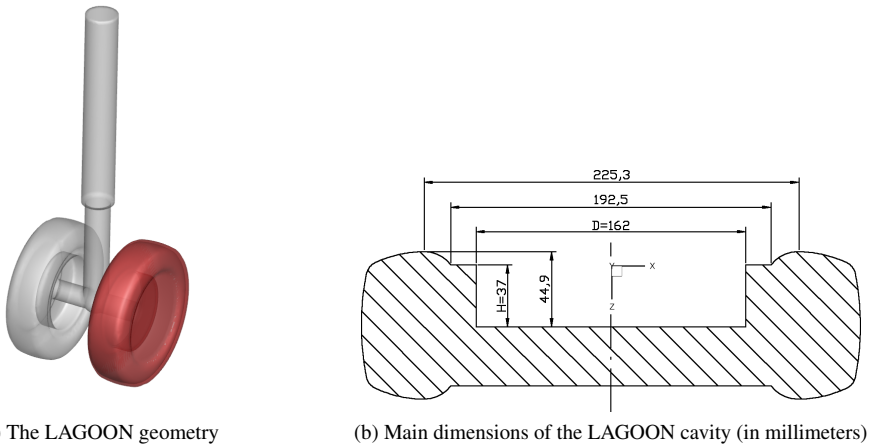

(a) The LAGOON geometry (b) Main dimensions of the LAGOON cavity (in millimeters)

Fig. 1 LAGOON geometry and cut of the isolated wheel in a median plane

2. Navier-Stokes setup

Computational domain and numerical resolution

The computational domain is a rectangular box of dimensions $(L_x, L_y, L_z) = (40D_w, 24D_w, 18D_w)$. In order to compute the turbulent flow around the wheel, ONERA's in-house code CEDRE [24] has been used to perform a Z-DES mode II [25] based on the one-equation turbulence model Spalart-Allmaras. A relaxation parameter has been applied on the boundaries in order to prevent any spurious reflexions on the boundaries of the computational domain. A 2nd order implicit Runge-Kutta temporal scheme has been used, coupled with a 2nd order HLLC flux scheme.

The upstream conditions are that of the LAGOON BANC-II problem statement in the CEPRA19 (ONERA's anechoic facility) configuration, namely $P_\infty = 96772.3Pa$, $T_\infty = 288.39K$, $\rho_\infty = 1.18kg/m^3$ and $M_\infty = 0.23$.

The calculation has been initialised with a RANS during 214ms before the Z-DES was launched. Then, after a Z-DES transient period, the flow has been solved for a total timelength of 328 ms with a time step $\Delta t_{CFD} = 5.10^{-6}s$, producing a total number of 65536 samples. Otherwise specified, all the signals considered in this study will have a duration of 328 ms. As for the computation of the power spectral densities, the Welch estimator will be used by windowing the blocks with a Hann function and averaging them to obtain a frequency resolution $\Delta f = 30Hz$.

Mesh description

In this study, two hybrid meshes $M1$ and $M2$ are considered. A cut of these two meshes in the median plane of the wheel is presented in figures 2a-2b. The $M1$ mesh is the one used in [17] and directly stems from the mesh that has been

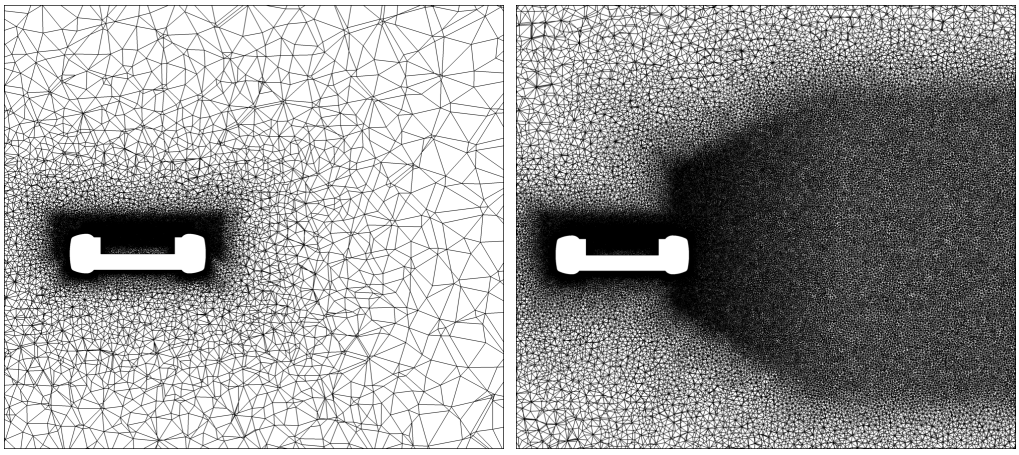

(a) $M1$ mesh (b) $M2$ Mesh

Fig. 2 Cut of $M1$ and $M2$ in a median plane of the wheel

used for the computation of the whole LAGOON gear in [26] which provided excellent results presented in the frame of the BANC [3]. It consists in a hybrid 15 million element (3.9 million nodes) mesh, including 3.7 million prisms (21 layers, with a first cell height of $D_w/\Delta = 30000$) devoted to solving the attached boundary layers. A volume refinement is defined in order to correctly reproduce the shear layer that detaches on the upstream part of the tyre. The cell size Δ corresponding to this refinement is such that $D_w/\Delta > 120$. This mesh has been designed with the idea that the flow at the direct vicinity of the wheel was mainly driven by the shear layer. It must be stressed that with the $M1$ mesh, the wake of the wheel is not resolved at all, as well as the flow on the external part of the cavity. The numerical resolution of the boundary layers is expected to give good results for the solid FW-H formulations. On the other hand, this mesh is expected to be poorly adapted to the permeable FW-H assessment as the resolution of the wake is very uncertain.

In this regard, a second mesh has been designed with emphasis on the accurate resolution of the wake of the wheel, as well as the correct propagation of the acoustic waves to the permeable surface. The second mesh $M2$ hence possesses exactly the same features than $M1$, except that, this time, the cell size downstream of the wheel allows an accurate resolution of the wake dynamics from the wheel to the endcap closure of the FW-H surface (a description of this surface will be given in the following paragraph).

The evolution of the cell diameter in the streamwise direction is depicted in figure 3. As we can see, the cell size has been roughly divided by 10 in the wake of the wheel from $M1$ to $M2$, hence giving a local cell size that ensures

the propagation of acoustic waves up to a frequency of about 5 kHz ($St_{D_w} = 19.3$) with negligible dissipation and dispersion errors.
Great care has been taken when choosing the cell stretching ratio in the streamwise direction in order not to generate spurious noise sources that would eventually be captured by the FW-H surface. This has led to a $M2$ mesh of 60 million elements (12.5 million nodes).

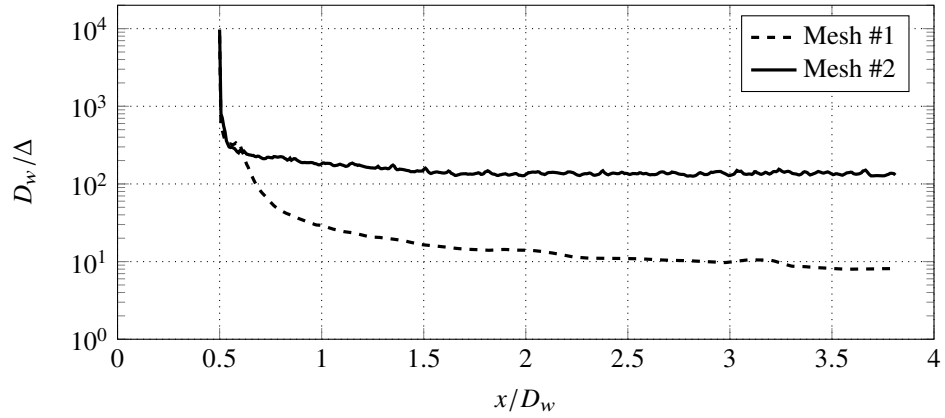

Fig. 3 Evolution of the ratio between the wheel diameter D_w and the local cell size Δ behind the wheel, at $y = 0$.

3. Ffowcs-Williams & Hawkings setup

ONERA's in-house code KIM [27] is used in this paper to compute the acoustic far-field. In this paragraph, we detail the setup of the FW-H calculations. In particular, the observation points, where the FW-H integral is computed are described. The design of the permeable surface is another crucial point that results from a trade-off between its discretisation (and eventually the memory cost associated) and its location relatively to the wake of the wheel as it is common that hydrodynamic perturbations crossing the surface induce spurious noise in the far field.

Observation surface

In all calculations, the observer points constitute a sphere of diameter $10D_w$. The center of this sphere coincides with the center of the wheel round cavity, in the plane grazing it. The whole sphere is composed of two half spheres, both having an azimuthal angle step $\Delta\theta = 10°$. The polar angle step is $\Delta\phi = 10°$ on the half sphere over the cavity, while the other half (underneath the cavity) has a polar angle step equal to $\Delta\phi = 11.5°$. The flow is directed towards $x > 0$, hence coming from $\theta = 0°$ while the direction $\phi = 0°$ corresponds to the pure flyover direction with respect to the cavity. The observation surface thus defined is presented in figure 4a.
In this paper, for the sake of clarity, only the results in the $\theta = 0°$ plane will be presented, as it is the plane that presents the most significant results. In a whole landing gear configuration, this would correspond to the pure sideline plane.

Integration surfaces

A closed surface containing the wheel and a part of its wake has been defined. Its design has been guided by the concern of minimizing the effects related to the wake that crosses it, as will be seen in the following paragraph. Consequently, this surface has a shape that follows approximately the expansion of the wake downstream of the wheel and extends to a distance of $3.81D_w$ from the wheel center. In the direction transverse to the flow, the dimension of the surface is $1.67D_w$. A cut of the permeable FW-H surface is presented in figure 4b, where the black dots correspond to numerical probes that will be used in the next paragraph for the assessment of the wake velocity and near-field pressure spectra.
In order to investigate the influence of the surface discretisation, two cases are defined: a fine surface, with rectangular surface elements of about $dS_F = 2.5.10^{-5}m^2$ in order to be as close as possible to the CFD mesh cell size, and a coarse one, obtained by coarsening the surface elements downstream of the wheel such as $dS_C = 16dS_F$ in the wake region, the wheel part being kept at the resolution dS_F.

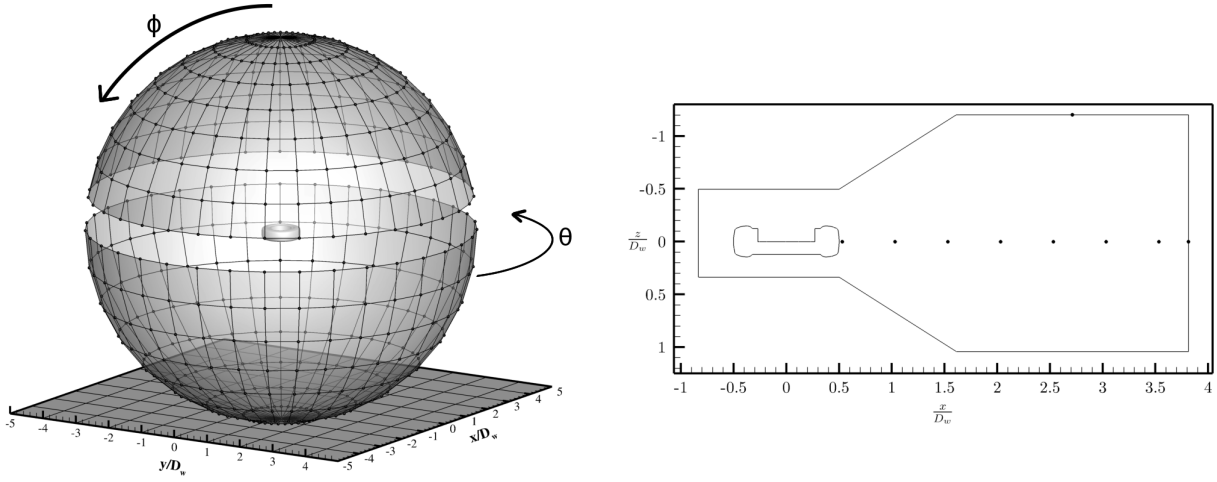

(a) Observation surface

(b) Permeable surface and numerical probes

Fig. 4 Description of the FW-H setup: observation surface (left) and permeable surface (right) used for the computation

B. Wake analysis on the $M2$ computation

A thorough analysis of the mean and unsteady flow results inside the cavity has already been carried out in [17] and will not be recalled here for the sake of brevity. This analysis allowed to conclude that the LAGOON shallow circular cavity behavior compares well with the literature of grazing cavities as for the development of the shear layer, as well as the wall pressure inside the cavity. The computation on the $M2$ mesh allows to complete this analysis with some results concerning the development of the wake downstream of the wheel. Please note that, in this subsection, the results presented have all been obtained on the $M2$ mesh.

In order to address the wake dynamics, seven numerical probes have been placed downstream of the wheel, all equally spaced of $0.5D_w$ from the location $x = 0.53D_w$ to $x = 3.53D_w$. An eighth probe has also been placed on the endcap closure of the FW-H surface at $x = 3.81D_w$. The power spectral densities of the transversal velocity v as well as the vertical velocity w are plotted in figure 5 as a function of the Strouhal number. As we can see, there is no evidence of a vortex-shedding like phenomenon in the wake of the wheel. The $f^{-5/3}$ canonical Kolmogorov power law in the inertial subrange has also been plotted for reference.

The mean streamwise velocity profile $\frac{\overline{U}}{U_\infty}$ has been plotted in spanwise and transverse cuts in figure 6 and allows to appreciate the decay of the wake inside the permeable surface (recall that the latter extends to $x^* = 3.81$). In particular, the mean velocity at $x^* = 3.81$ is about 10% of the upstream velocity. A slight asymmetry that tends to vanish with the distance is visible in the transverse direction in figure 6b (note that the $z > 0$ direction is oriented towards the inside of the cavity). The maximum velocity is obtained over the wheel (negative z values), where the recirculation inside the cavity takes place.

In order to assess the pressure field in the vicinity of the wake, a probe has been placed on the upper surface of the FW-H surface at the location $x/D_w = 2.71$ and at a vertical distance of $1.2D_w$ from the cavity floor. The PSD of the pressure is plotted in figure 7 and shows a wide emergence at 1850 Hz in the $M2$ computation that could hardly be detected on the $M1$ computation. This figure allows to appreciate how the $M2$ mesh has improved the propagation of the sound waves around the wake of the wheel compared to the $M1$ case. In particular, the CFD mesh cut-off seems here to be slightly greater than the 5 kHz announced in the first section.

The crossing of the surface by hydrodynamic fluctuations is known to generate spurious noise in the far-field when the permeable FW-H equation is considered. The RMS levels of the pressure on the endcap closure of the FW-H surface are represented in figure 8 in order to quantify this phenomenon. As we can see, only a small fraction of this surface is affected by significant RMS levels that may pollute the solution in the far-field. Among the two principal spots of high RMS levels, we can see that the most intense corresponds to positive values of z, ie under the wheel.

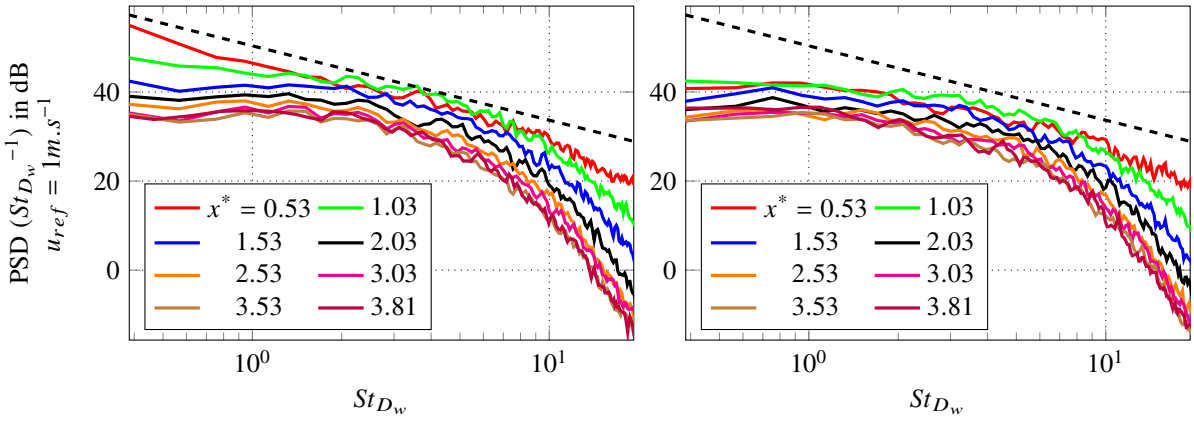

(a) Power spectral density of the transverse v velocity

(b) Power spectral density of the vertical w velocity

Fig. 5 Power spectral density of the transverse velocity components at eight x/D_w locations in the wake. Dashed black line: Kolmogorov's power law $f^{-5/3}$

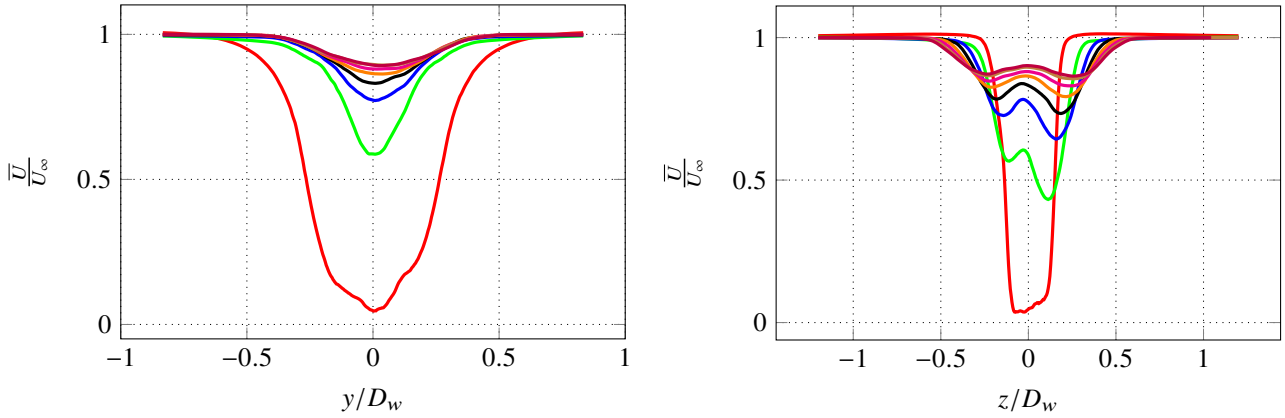

(a) Mean streamwise velocity deficit in the (yOx) plane

(b) Mean streamwise velocity deficit in the (zOx) plane

Fig. 6 Mean streamwise velocity profiles in spanwise and transverse cuts of the wake $x^* = 0.53$: (——), $x^* = 1.03$: (——), $x^* = 1.53$: (——), $x^* = 2.03$: (——), $x^* = 2.53$: (——), $x^* = 3.03$: (——), $x^* = 3.53$: (——), $x^* = 3.81$: (——)

IV. Far-Field Acoustics

In this section, the FW-H equation is first recalled and a brief description of its terms is made. Then, the effect of the time signal length is assessed in order to prove the convergence of the spectra that are shown in all the rest of the paper. Finally, the results of the FW-H calculation are presented for different configurations and discussed.

A. The Ffowcs-Williams & Hawkings equation

The process by which the energy carried by a turbulent flow is converted to acoustic perturbations is described by the Lighthill equation. This equation is obtained by rearranging the Navier-Stokes equations into an inhomogeneous wave equation that can then be solved with the Green's functions formalism. This methodology forms the basis of an acoustic analogy. By using an acoustic analogy, one thus avoids the high computational cost necessary to accurately propagate sound waves to the far-field without too much dissipation and dispersion. Ffowcs-Williams & Hawkings [7] have then extended this methodology to account for the presence of moving surfaces in the flow. Let $(\Sigma : f = 0)$ be a mathematical surface enclosing the body of interest, such as $f < 0$ inside the surface, $f > 0$ outside and $\vec{\nabla} f = \vec{n}$. The surface is moving with respect to the reference frame at a velocity $\vec{v}^{\Sigma}$ and the flow velocity is $\vec{u}$. After the developments

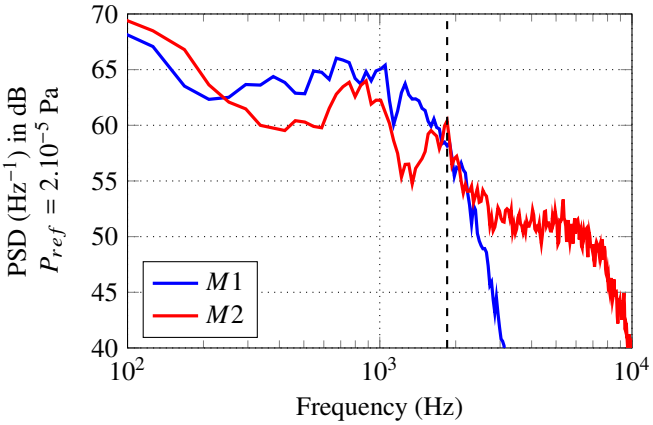

Fig. 7 Power spectral density of the CFD pressure time signal for an observer located at $x* = 2.71$ and at a vertical distance $1.2D_w$ from the cavity floor. The dashed line indicates $f = 1850Hz$

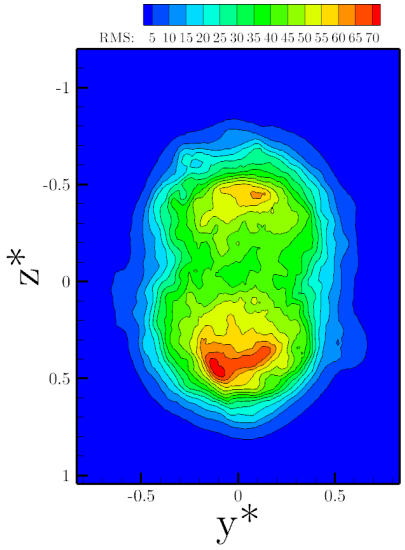

Fig. 8 Root mean square iso-contours of the pressure on the endcap closure of the FW-H surface

of Di Francescantonio [28] that allow the surface to be permeable, the FW-H equation writes:

$$\Box^2 \left[c^2(\rho - \rho_\infty)H(f)\right] = \frac{\partial}{\partial t}\left[\rho_\infty U_n \delta(f)\right] - \frac{\partial}{\partial x_i}\left[L_i \delta(f)\right] + \frac{\partial^2}{\partial x_i \partial x_j}\left[T_{ij} H(f)\right]$$

where

$$U_n = u_n + \left[(\rho/\rho_\infty) - 1\right](u_n - {v_n}^\Sigma)$$
$$L_i = P'_{ij} n_j + \rho u_i (u_n - {v_n}^\Sigma)$$
$$T_{ij} = P'_{ij} + \rho u_i u_j - c^2(\rho - \rho_\infty)\delta_{ij}$$
$$P'_{ij} = p'\delta_{ij} - \tau_{ij}$$

The solution can be analytically expressed by convolution with the free-space 3D Green's function and thus writes:

$$4\pi c^2(\rho - \rho_\infty)H(f) = \frac{\partial^2}{\partial x_i \partial x_j}\int_{V_{(f>0)}} \underbrace{\frac{\left[T_{ij}\right]_{ret}}{r|1 - M_r|}}_{\text{(a)}} dV - \frac{\partial}{\partial x_i}\int_\Sigma \underbrace{\frac{[L_i]_{ret}}{r|1 - M_r|}}_{\text{(b)}} dS + \frac{\partial}{\partial t}\int_\Sigma \underbrace{\frac{\rho_\infty [U_n]_{ret}}{r|1 - M_r|}}_{\text{(c)}} dS$$

where $[]_{ret}$ means that the time-dependant variable inside the brackets is evaluated at the retarded time $\tau_{ret} = t - \frac{r}{c_0}$, r being the source-observer distance.

The calculation of the far-field acoustic pressure requires the evaluation of the three integrals described previously, that are respectively known as:

(a) : the volumic quadrupolar source term that accounts for the noise generated by the turbulence itself, ie the time variation of the vorticity in the regions of strong shear,

(b) : the surface loading source term that describes the noise generated by the interaction between turbulent fluctuations and solid boundaries of the moving body,

(c) : the surface thickness term related to the kinematics of the body.

This equation has been derived from the Navier-Stokes equations without any loss of generality, under the assumption that the acoustic perturbations and the flow are not coupled. The major drawback is then the computational cost associated with the evaluation of the Lighthill stress tensor T_{ij} in the volume exterior to the integration surface. While it is theoretically possible to compute the (a) term outside of the integration surface defined in the first section, the computational cost required is completely out of reach for industrial applications. In practice, two approaches are then possible.

- The first, and the most commonly used, is known as the *solid* formulation of the FW-H equation. The basic idea is to take the surface Σ coincident with the solid boundaries of the body considered so that only the pressure has to be saved on the rigid walls. Plus, two assumptions are made: the walls are impermeable and non-vibrant, and the Lighthill stress tensor is negligible everywhere. If these two assumptions are made, then the FW-H equation reduces to the Curle equation [29] and the computational cost is significantly reduced. This formulation is then very convenient for industrial applications but one has to be careful that the assumptions made are valid when employing it.
- The second approach is to design the Σ control surface so as it contains the body and all the most turbulent regions. The idea is that the Lighthill stress tensor vanishes outside the integration surface, so that the $\int_{V(f>0)}$ term can be discarded. This actually results in a Kirchoff-like integration, provided that the flow leaving the surface on its endcap closure is not too strong, so the surface can be considered in the linear region. It has been suggested that the quadrupolar sources crossing the surface might be chopped into two dipoles that are much more efficient acoustically [11], and the one inside the surface would eventually cause spurious noise generation. Several authors have derived corrective terms based on the calculations of the Lighthill source term flux across the surface in order to mitigate this phenomenon [30, 31]. Another idea brought by Shur et al. [32] consists in averaging several outflow surfaces in order to remove the hydrodynamic component from the integration. These methods, however, have not been assessed in the present study but this constitutes an interesting perspective for landing gear noise as they have mainly been used for jet and trailing edge noise.

In this paper, the solid and permeable formulations are alternatively considered in order to compare the results they provide at a typical landing Mach number of 0.23 and to assess the contribution of the quadrupolar sound.

B. Convergence of the spectra

First, three timelengths have been considered to compute the solid FW-H integral with the wall pressure perturbations obtained with the $M1$ mesh configuration in order to check the convergence of the spectra that will be presented in the rest of the paper. These three timelengths are hereafter referred to as T_1, T_2, and T_3 and equal respectively to 33.25, 85.20 and 118.45 T_{D_w} where $T_{D_w} = \frac{D_w}{U_\infty}$. The spectra at the location ($\theta = 0°, \phi = 30°$) (that is, 30° upstream from the flyover direction) are plotted in figure 9 where the dashed vertical line corresponds to a frequency $f = 1571Hz$. As we can see, increasing the integration time has allowed a more tonal behavior to be detected at 1.5 kHz than what was stated in the previous paper [17]. It should be highlighted that, even if the extension of the integration time length has led to a peakier spectrum, the latter still remains far from the classical tones usually observed in academic cavity studies, as the peak is still 400 Hz wide. This is consistant with the study made by Marsden et al. [22] who state that no strong acoustic tone can be generated in cavities with depth to diameter ratio such as $\kappa \leq 1$.

The T_3 spectrum is almost identical to the T_2 one for frequencies higher than 200 Hz, hence showing that a $T_2 = 328ms$ integration time is enough in the present case.

We suppose that this conclusion holds for the permeable formulation and for all the observation points and, from now on, a timelength of 328 ms will be used in the following subsections.

In what follows, unless specified, all the spectra and integrated levels will be considered in the [200; 5000]Hz interval. The lower bound of this interval is thus limited to 200 Hz by the available 328 ms of time signals, and the upper bound

by the CFD mesh cut-off frequency indicated in the first section.

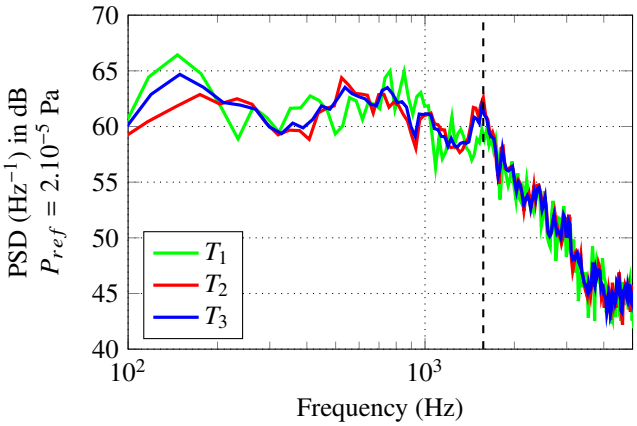

Fig. 9 Spectrum of the far-field pressure signal computed with a solid FW-H at the position ($\theta = 0°$, $\phi = 30°$) for three different recorded time signal durations: 128ms, 328ms and 456ms

C. Results

1. Solid formulation: $M1$ vs $M2$

The aim of this paragraph is to study how an accurate resolution of the wake downstream of a bluff body influences the results obtained with the solid FW-H formulation. In this regard, the results obtained with the solid formulation in the case of the $M1$ and $M2$ computations will be compared. The surface mesh over the rigid walls has a similar resolution in both cases. The only difference between $M1$ and $M2$ is the refinement downstream of the wheel that allows an accurate resolution of the wake.

The results at four observation points in the median plane are plotted in figures 10-11. The overall agreement is satisfying but, still, several observations can be made.

First, the 1.5 kHz peak is equally well recovered in the direction $\phi = 30°$ (see fig. 10b). As already pointed out in [17], the most plausible explication for the occurrence of this tone is a coupling between a depth mode of the circular cavity and a Rossiter mode. This phenomenon is expected to be mainly driven by the shear layer, which is already accurately described by the $M1$ mesh.

Another interesting point is that the noise predictions are in very good agreement in all directions except the ones parallel to the flow (figs 10a-11b) where a difference of several dB can be observed in the high-frequency range (typically, for $f \geq 2kHz$).

Finally, we can observe that the 1850 Hz pseudo-tone already observed over the wake in the previous section in figure 7 is better described by the $M2$ computation (see figure 11) for downstream observers.

These observations allow us to conclude that the overall effect of resolving the wake on the acoustic predictions is small with the solid formulation of the FW-H equation. The differences here are mainly in the high-frequency range, and in the upstream direction. This is further confirmed by the overall sound pressure levels (OASPL) calculated between 200 Hz and 5 kHz and presented in figure 12. It should as well be stressed that the differences in the integrated levels are of about 2 dB at most and occur for observation angles that are of limited interest for industrial applications. The results obtained with the solid formulation on the $M1$ and $M2$ meshes seem to indicate that accurately resolving the wake gives very similar results in both cases, except in the upstream direction, where a slight overestimation of the levels is found with the coarse mesh. A possible explanation for this difference could be the generation of a spurious noise source due to a too sudden coarsening of the CFD mesh downstream of the wheel. This source could then induce spurious wall pressure perturbations that would eventually appear in the FW-H integral. This seems to indicate that, even if the quadrupolar sources are neglected, one still has to be careful about the resolution of the wake, and in particular, about the stretching ratio imposed during the mesh generation process.

At this stage, the quadrupolar contribution of the sound is still unknown as the permeable formulation has not been used. The aim of the next paragraph is to compare the results obtained with the solid and the permeable formulations.

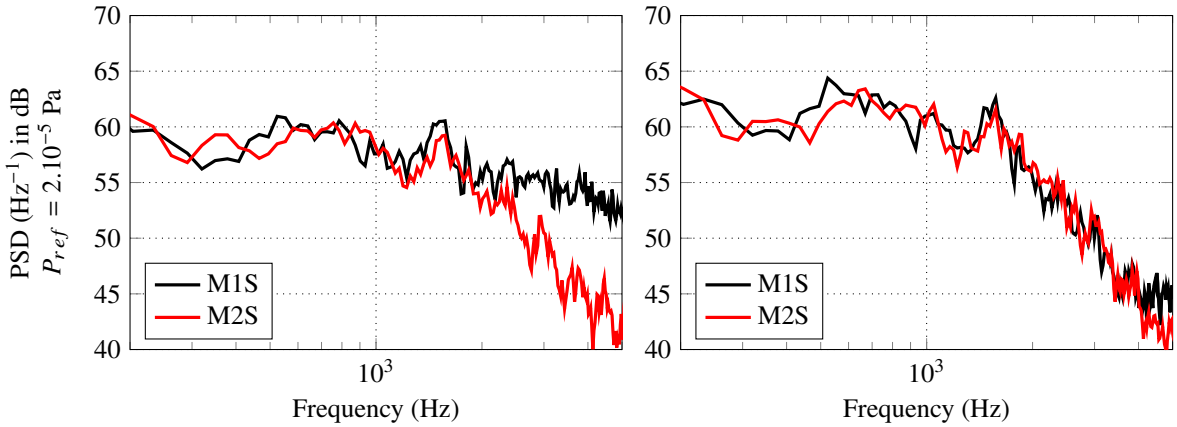

(a) Microphone ($\theta = 0°; \phi = 80°$)

(b) Microphone ($\theta = 0°; \phi = 30°$)

Fig. 10 Spectrum of the far-field pressure signal computed at two positions in the upstream direction with the *solid* formulation of the FW-H equation

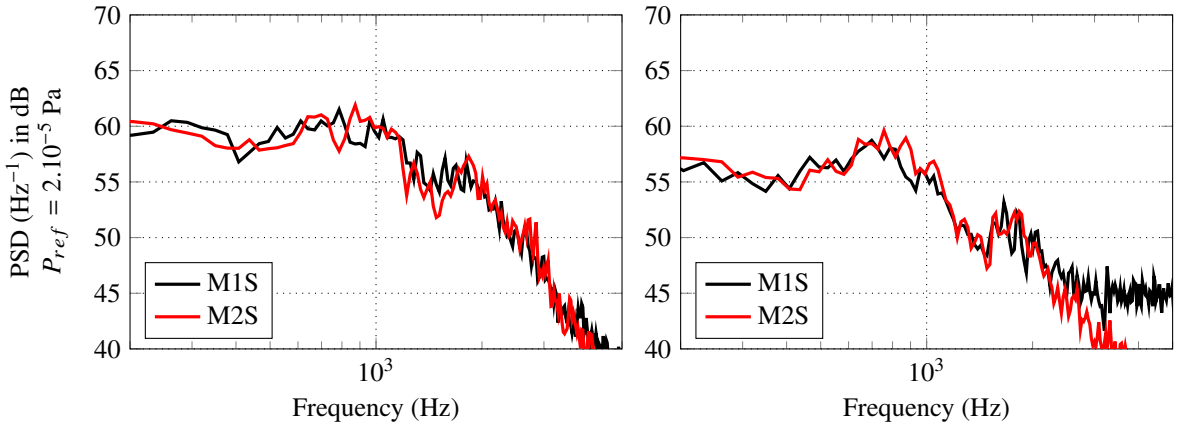

(a) Microphone ($\theta = 0°; \phi = 330°$)

(b) Microphone ($\theta = 0°; \phi = 280°$)

Fig. 11 Spectrum of the far-field pressure signal computed at two positions in the downstream direction with the *solid* formulation of the FW-H equation

2. Closed surface - Influence of the FW-H surface resolution

In this paragraph, the FW-H equation is used in its permeable formulation with the downstream closure kept closed. The aim of this paragraph is twofold. Firstly, the comparison between the permeable and solid results should allow to conclude on the contribution of the wake quadrupoles to the total radiated noise. Secondly, the cell size of the integration surface is a parameter that is rarely mentioned in the litterature. Consequently, the surface introduced in the first section is divided into two cases. The first surface has a spatial resolution such that each point is located approximately $5mm$ away from its neighbours, resulting in surface elements of about $dS = 2.5.10^{-5}m^2$. The second surface has been obtained by coarsening the first one downstream of the wheel to obtain a distance of about $20mm$ between each point of the grid, thus resulting in surface elements of about $dS = 4.10^{-4}m^2$. The results obtained with these surfaces will be referred to as $M2C\text{-}Cl$ (Mesh2-Coarse-Closed) for the coarse surface, and $M2F\text{-}Cl$ (Mesh2-Fine-Closed) for the finer one. The same observation points as in the previous paragraph are considered and the spectra in the far-field are presented in figures 13 - 14, where the $M2S$ results are also plotted for the sake of comparison.

The results obtained in the $M2C\text{-}Cl$ configuration exhibit unphysically higher levels compared to the solid $M2S$ configuration. The difference between these two configurations is shown to increase when the observation point

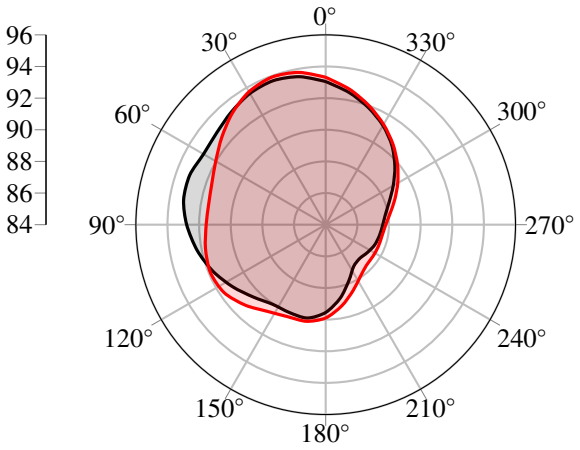

Fig. 12 OASPL (dB) for the solid FW-H computation on (——) $M1$ mesh and (——) $M2$ mesh in the (zOx) plane

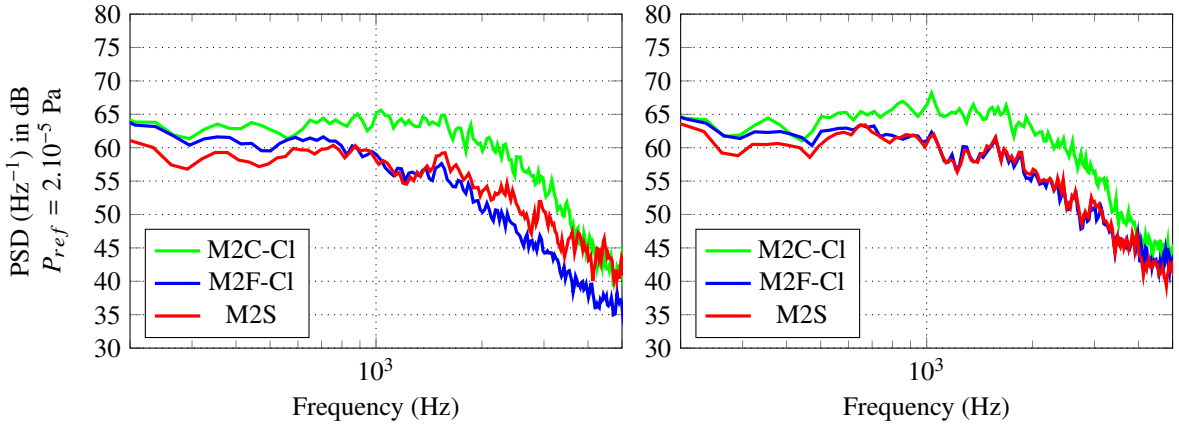

(a) Microphone ($\theta = 0°; \phi = 80°$)

(b) Microphone ($\theta = 0°; \phi = 30°$)

Fig. 13 Spectrum of the far-field pressure signal computed at two positions in the upstream direction with a closed integration surface

considered gets closer to the downstream direction. This phenomenon has already been described by numerous authors in the aeroacoustic community and is most likely due to the crossing of the endcap surface by the wake of the wheel. Curiously, apart from small downstream observation angles, the $M2F\text{-}Cl$ results agree very well with the the $M2S$ results although the surface remains closed at its downstream section, the only different parameter between $M2C\text{-}Cl$ and $M2F\text{-}Cl$ being the FW-H surface elements size on the integration surface.

The OASPL has been computed in the median (zOx) plane and is plotted in figure 15. This figure allows to appreciate how increasing the resolution of the FW-H surface yields results in much better agreement with the $M2S$ computation. Still, discrepancies appear and grow as the observer direction gets close to downstream angles. The OASPL in the $M2F\text{-}Cl$ configuration are slightly higher than those obtained with the solid formulation. As we can notice in figures 13 and 14, the agreement between the $M2S$ and $M2F\text{-}Cl$ cases is good (less than 2 dB) for observation angles $\phi < 200°$ and $\phi > 310°$. This asymmetry echoes the one already observed in figure 8, although the link is not straightforward.

Finally, the comparison between the $M2S$ and the $M2F\text{-}Cl$ results seems to indicate that the quadrupolar sources in the wake of this isolated landing gear wheel have a negligible amplitude under 5kHz, the differences with the $M2S$ results being attributed to the crossing of the integration surface by the wake, rather than a quadrupolar contribution. As highlighted in figure 15a, the surface discretisation has a major effect on the far-field results as it increases the integrated

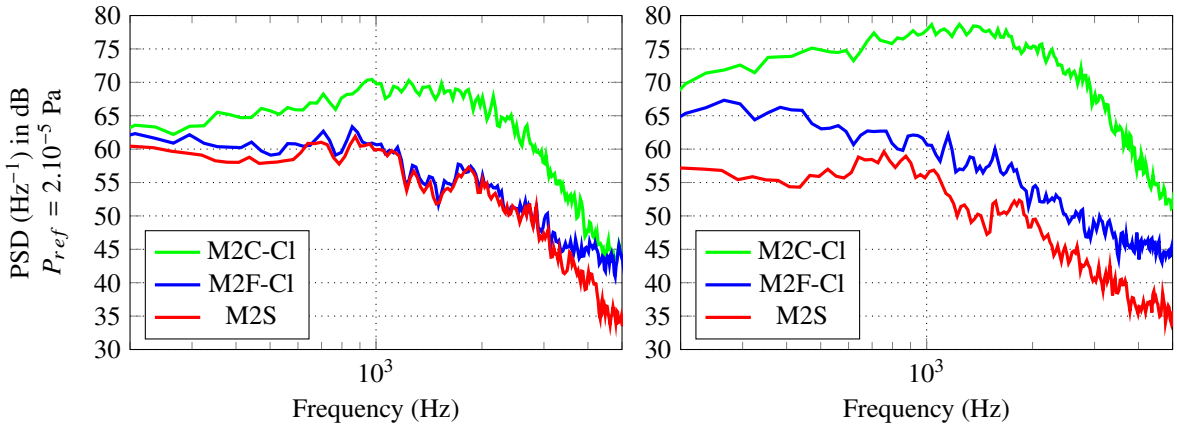

(a) Microphone ($\theta = 0°; \phi = 330°$)

(b) Microphone ($\theta = 0°; \phi = 280°$)

Fig. 14 Spectrum of the far-field pressure signal computed at two positions in the downstream direction with a closed integration surface

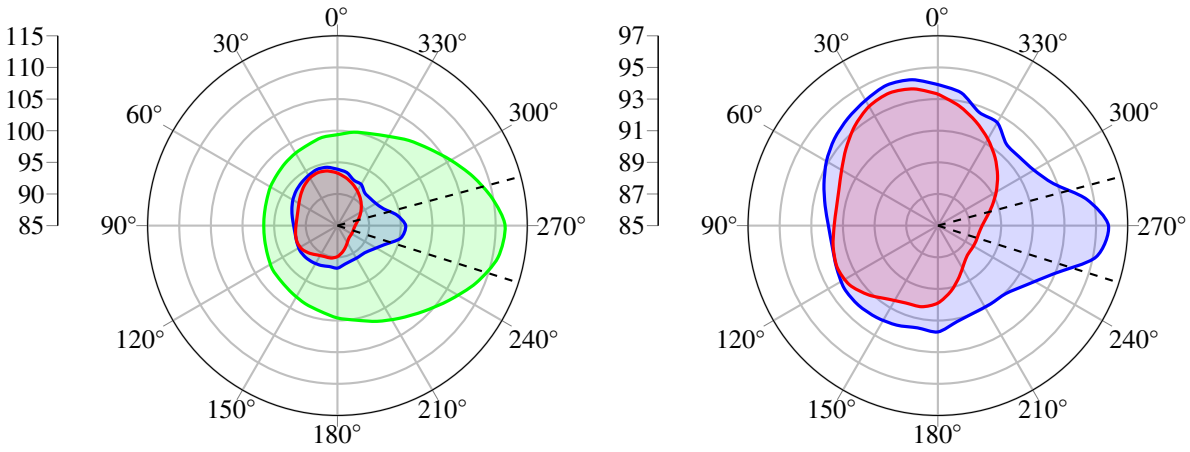

(a) M2C-Cl vs M2F-Cl vs M2S

(b) M2F-Cl vs M2S

Fig. 15 OASPL (dB) for the (——) $M2S$ FW-H computation, (——) $M2C$-Cl, and (——) $M2F$-Cl in the (zOx) plane. The dashed lines represent the angle covered by the outflow surface

levels by at least 3 dB in every direction.

3. Influence of opening the endcap closure of the surface

In the previous paragraph, the discretisation of the FW-H surface has been varied from a coarse resolution to a finer one ($dS_C = 16dS_F$), which has allowed the far-field results to fall in much better agreement with the solid results for the fine resolution, except in the downstream direction. The coarse FW-H surface, on the other hand, has led to unphysically high noise levels in all directions. The aim of this paragraph is to further investigate this phenomenon by opening the downstream endcap of the FW-H surface in the $M2C$ and $M2F$ configurations. The cases thus defined will be referred to as $M2C$-Op and $M2F$-Op respectively.

The results are plotted in figures 16 - 17 and show that, with an open downstream section, the coarse and fine FW-H surfaces exhibit almost exactly the same results (with differences of less than 1dB). As for the $M2F$-Cl configuration, the spectra fall in very good agreement with the $M2S$ configuration, except at low frequency ($f \leq 400Hz$) and in the flow direction where the discrepancies are very high (figure 17b). Here, the fact that the $M2F$-Op and $M2C$-Op

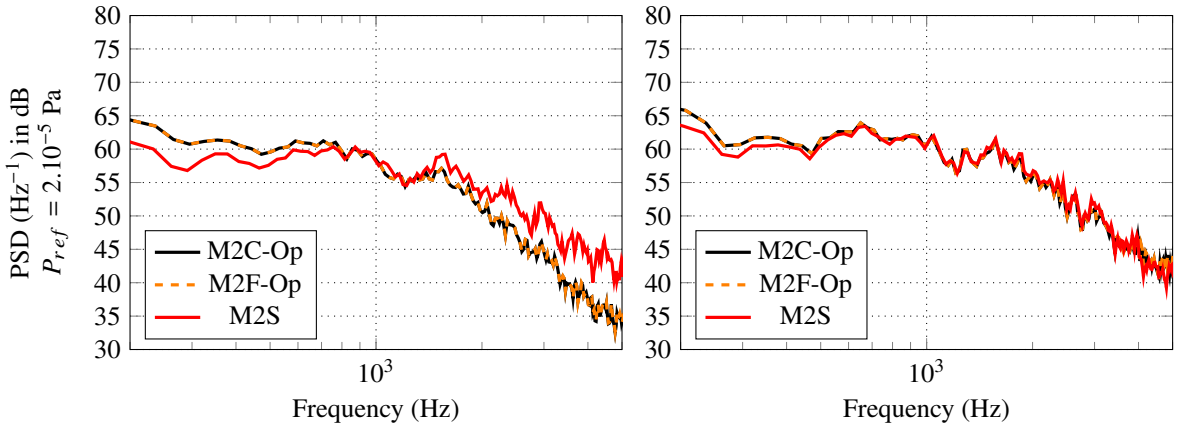

(a) Microphone ($\theta = 0°; \phi = 80°$)

(b) Microphone ($\theta = 0°; \phi = 30°$)

Fig. 16 Spectrum of the far-field pressure signal computed at two positions in the upstream direction with an open integration surface

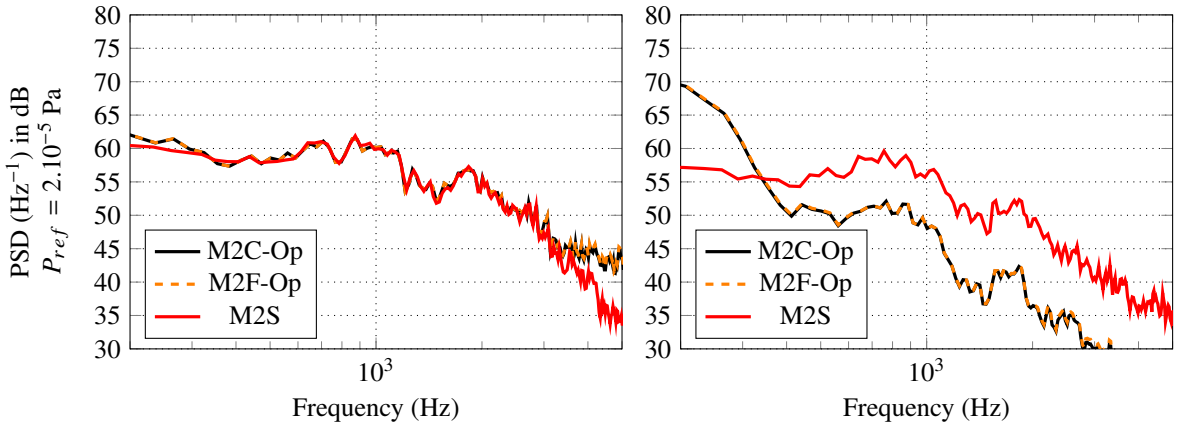

(a) Microphone ($\theta = 0°; \phi = 330°$)

(b) Microphone ($\theta = 0°; \phi = 280°$)

Fig. 17 Spectrum of the far-field pressure signal computed at two positions in the downstream direction with an open integration surface

configurations yield almost exactly the same results allows to conclude that the effect of the surface discretisation on noise predictions is actually very localised on the downstream section of the integration surface.
To summarize, the OASPL have been plotted for all the cases in figure 18. Coarsening the FW-H integration surface has, in the present case, very little influence on the integrated levels when the downstream end is open. This seems to indicate that the key parameter is, not only the crossing of the surface by the wake, but more precisely the discretisation of the surface closure and suggests the existence of a link between the size of the structures and the surface elements involved in the calculation of the FW-H integral.

A snapshot of the fluctuating density is plotted on the coarse surface (figure 19a) and on the fine surface (figure 19b) to illustrate this phenomenon. It is clear that the turbulent structures are way better described on the fine surface than on the coarse one where artifacts in the integration process are likely to appear in the far-field due to the undersampling of the downstream surface. Further work will focus on determining the precise implications of the surface discretisation on the numerical calculation of the FW-H surface integrals.

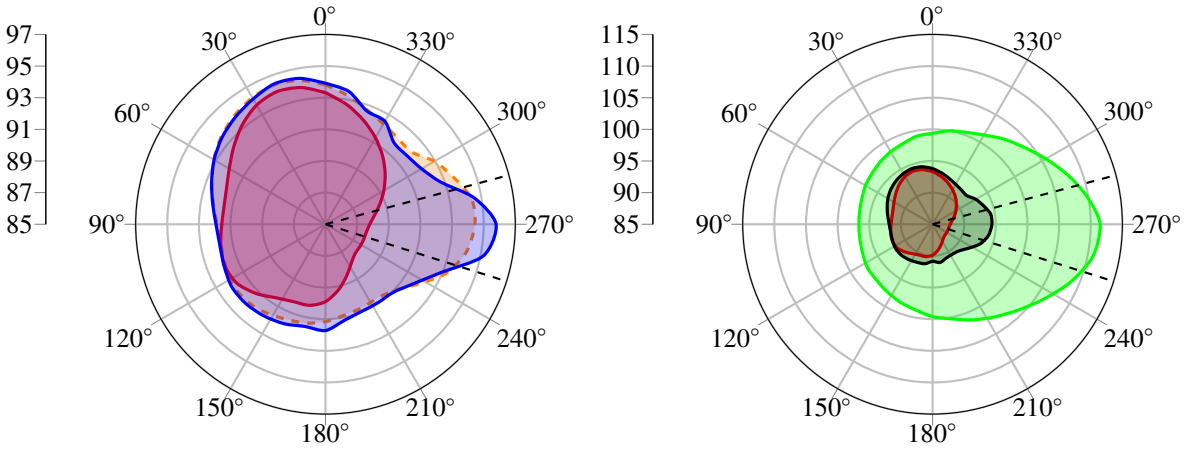

(a) Fine integration surface (b) Coarse integration surface

Fig. 18 Effect of opening the downstream end of the surface on the OASPL (dB) for the (——) $M2S$ FW-H computation, (- - -) $M2F$-Op and (——) $M2F$-Cl (on the left), (——) $M2C$-Cl and (——) $M2C$-Op (on the right) in the (zOx) plane. The dashed lines represent the angle covered by the outflow surface

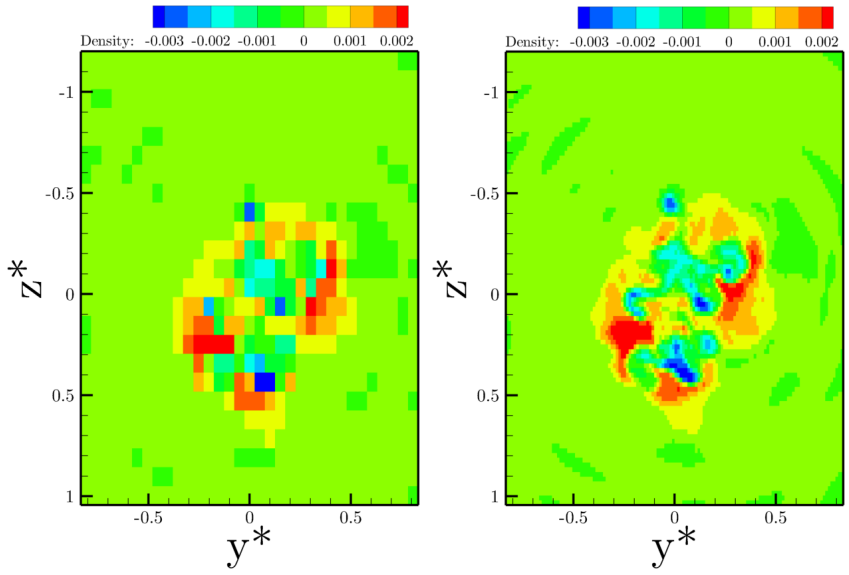

(a) Coarse endcap (b) Fine endcap

Fig. 19 Snapshot of the fluctuating density ρ' on the downstream closure of the FW-H integration surface

V. Conclusions

The far-field acoustic radiation generated by an isolated landing gear wheel from the LAGOON configuration has been addressed with a hybrid method. First, the turbulent flow field surrounding the wheel has been computed by means of a Zonal Detached Eddy Simulation that allowed to accurately solve the shear layer over the shallow round cavity of the wheel. A second mesh has been designed to additionally resolve the wake of the wheel and investigate the contribution of the quadrupolar volumic sources to the far-field.

The wheel cavity has shown to behave like an academic cylindrical cavity as for the development of the shear layer and the pressure signature inside the cavity. The wake downstream of the wheel has also been addressed on an appropriate mesh $M2$ and it has been shown that no vortex-shedding mechanism occurs downstream of the wheel. As the crossing of the FW-H closure is known to cause some problems related to the wake of the body, the mean profile of the streamwise

velocity has been scrutinised and it has been shown that the wake strength is considerably reduced on the endcap closure of the FW-H surface as the mean streamwise velocity deficit is under 10% of the free-stream velocity on the downstream end of the FW-H surface.
The FW-H computations with the solid formulation have first been carried on with the $M1$ and $M2$ meshes. It has been shown that the overall agreement between the two computations is very satisfying, except in the upstream direction where the $M1$ computation tends to give slightly higher noise levels, most likely due to a too sudden coarsening of the mesh downstream of the wheel. This suggests that, even when using the FW-H in its solid formulation, one has to be cautious when meshing the wake in order to improve the accuracy of the noise predictions, specially for low observation angles relative to the flow.
The permeable formulation has been assessed by keeping the endcap closure of the FW-H surface and varying its discretisation. This has led to the conclusion that the discretisation of the downstream closure of the surface seems to be a parameter that greatly influences the noise predictions. In this study, it has been found that refining the surface elements involved in the surface integral has allowed an almost perfect match with the solid formulation results over a large frequency interval, while the coarsely meshed surface closure generates spurious noise in every direction. Some discrepancies remain though, particularly at very low frequencies and in the directions close to the streamwise direction. The endcap closure of the surface has then been removed from the calculation. This has greatly improved the results obtained with the coarse integration surface, that were shown to match perfectly that of the fine integration surface with endcap open. However, as previously, opening the downstream surface induces discrepancies at low frequency and in the flow direction.
The very good agreement between the solid and permeable results seems to indicate that the quadrupolar volumic source is negligible for the considered Mach number $M = 0.23$ and for frequencies under 5kHz (the CFD mesh cut-off frequency in the present case). The contribution of the quadrupolar noise relatively to the other terms decreases with the Mach number. We can then expect the solid formulation of the FW-H equation to give accurate results for Mach numbers between 0.18 and 0.23. This is a valuable result for landing gear noise predictions, as the computational cost (memory and CPU) related to the computation of the far-field pressure is significantly reduced by using this formulation.

References

[1] Fink, M. R., "Airframe noise prediction method," Tech. rep., United Technologies Research Center East Hartford CT, 1977.

[2] Guo, Y., "A statistical model for landing gear noise prediction," *Journal of Sound and Vibration*, Vol. 282, No. 1, 2005, pp. 61–87.

[3] de la Puente, F., "Aeroacoustic simulations of landing gears with unstructured grids and a ZDES turbulence model," Ph.D. thesis, University Pierre et Marie curie - Paris 6, 2017.

[4] Casalino, D., Ribeiro, A. F., Fares, E., and Nölting, S., "Lattice–Boltzmann aeroacoustic analysis of the LAGOON landing-gear configuration," *AIAA journal*, Vol. 52, No. 6, 2014, pp. 1232–1248.

[5] Murayama, M., Yokokawa, Y., Yamamoto, K., and Hirai, T., "Computational study of low-noise fairings around tire-axle region of a two-wheel main landing gear," *Computers & Fluids*, Vol. 85, 2013, pp. 114–124.

[6] Spalart, P. R., Shur, M. L., Strelets, M. K., and Travin, A. K., "Initial noise predictions for rudimentary landing gear," *J. Sound and Vib.*, Vol. 330, No. 17, 2011, pp. 4180–4195.

[7] Williams, J. F., and Hawkings, D. L., "Sound generation by turbulence and surfaces in arbitrary motion," *Philosophical Transactions of the Royal Society of London*, Vol. 264, No. 1151, 1969, pp. 321–342.

[8] Mendez, S., Shoeybi, M., Lele, S., and Moin, P., "On the use of the Ffowcs Williams-Hawkings equation to predict far-field jet noise from large-eddy simulations," *International Journal of Aeroacoustics*, Vol. 12, No. 1-2, 2013, pp. 1–20.

[9] Spalart, P. R., "On the precise implications of acoustic analogies for aerodynamic noise at low Mach numbers," *J. Sound and Vib.*, Vol. 332, No. 11, 2013, pp. 2808–2815.

[10] Souliez, F., Long, L., Morris, P., and Sharma, A., "Landing Gear Aerodynamic Noise Prediction Using Unstructured Grids," *International Journal of Aeroacoustics*, Vol. 1, No. 2, 2002, pp. 115–135. doi:10.1260/147547202760236932.

[11] Greschner, B., Thiele, F., Jacob, M. C., and Casalino, D., "Prediction of sound generated by a rod–airfoil configuration using EASM DES and the generalised Lighthill/FW-H analogy," *Computers & fluids*, Vol. 37, No. 4, 2008, pp. 402–413.

[12] Jacob, M. C., Boudet, J., Casalino, D., and Michard, M., "A rod-airfoil experiment as a benchmark for broadband noise modeling," *Theoretical and Computational Fluid Dynamics*, Vol. 19, No. 3, 2005, pp. 171–196.

[13] Liu, W., Kim, J. W., Zhang, X., Angland, D., and Caruelle, B., "Landing-gear noise prediction using high-order finite difference schemes," *J. Sound and Vib.*, Vol. 332, No. 14, 2013, pp. 3517–3534.

[14] Casalino, D., Ribeiro, A. F., and Fares, E., "Facing rim cavities fluctuation modes," *Journal of Sound and Vibration*, Vol. 333, No. 13, 2014, pp. 2812–2830.

[15] Wang, M., Angland, D., and Zhang, X., "The noise generated by a landing gear wheel with hub and rim cavities," *J. Sound and Vib.*, Vol. 392, No. Supplement C, 2017, pp. 127 – 141.

[16] Wang, M., Angland, D., and Scotto, A., "Interaction Noise from Tandem Landing Gear Wheels with Hub and Rim Cavities," *23rd AIAA/CEAS Aeroacoustics Conference, AIAA paper 2017-3014*, 2017, p. 3014.

[17] De La Puente, F., Sanders, L., Druault, P., and Vuillot, F., "Investigation on landing gear shallow round cavity flow field and noise signature," *22nd AIAA/CEAS Aeroacoustics Conference, AIAA paper 2016-2774*, 2016, p. 2774.

[18] Ma, Z., Zhang, X., Smith, M., and Sanderson, M. R., "Aerodynamic and Acoustic Measurements of a Single Landing Gear Wheel," *19th AIAA/CEAS Aeroacoustics Conference*, 2013, p. 2160.

[19] Manoha, E., Bulté, J., and Caruelle, B., "LAGOON: an experimental database for the validation of CFD/CAA methods for landing gear noise prediction," *14th AIAA/CEAS Aeroacoustics Conference, AIAA paper 2008-2816*, 2008, p. 2816.

[20] Manoha, E., Bulté, J., Ciobaca, V., and Caruelle, B., "LAGOON: further analysis of aerodynamic experiments and early aeroacoustics results," *15th AIAA/CEAS Aeroacoustics Conference, AIAA paper 2009-3277*, 2009, p. 3277.

[21] Manoha, E., and Caruelle, B., "Summary of the LAGOON solutions from the Benchmark problems for Airframe Noise Computations-III Workshop," *21st AIAA/CEAS Aeroacoustics Conference AIAA paper 2015-2846*, 2015.

[22] Marsden, O., Bailly, C., Bogey, C., and Jondeau, E., "Investigation of flow features and acoustic radiation of a round cavity," *Journal of Sound and Vibration*, Vol. 331, No. 15, 2012, pp. 3521–3543.

[23] Block, P. J., "Noise response of cavities of varying dimensions at subsonic speeds," 1976.

[24] Refloch, A., Courbet, B., Murrone, A., Villedieu, P., Laurent, C., Gilbank, P., Troyes, J., Tessé, L., Chaineray, G., Dargaud, J., et al., "CEDRE software," *AerospaceLab*, , No. 2, 2011, pp. p–1.

[25] Deck, S., "Recent improvements in the Zonal Detached Eddy Simulation (ZDES) formulation," *Theoretical and Computational Fluid Dynamics*, Vol. 26, No. 6, 2012, pp. 523–550. doi:10.1007/s00162-011-0240-z.

[26] de la Puente Cerezo, F., Sanders, L., Vuillot, F., Druault, P., and Manoha, E., "Zonal Detached Eddy Simulation of a simplified nose landing-gear for flow and noise predictions using an unstructured Navier-Stokes solver," *Journal of Sound and Vibration*, Vol. 405, 2016, pp. 86 – 111.

[27] Prieur, J., and Rahier, G., "Aeroacoustic integral methods, formulation and efficient numerical implementation," *Aerospace Science and Technology*, Vol. 5, No. 7, 2001, pp. 457–468.

[28] Di Francescantonio, P., "A new boundary integral formulation for the prediction of sound radiation," *Journal of Sound and Vibration*, Vol. 202, No. 4, 1997, pp. 491–509.

[29] Curle, N., "The influence of solid boundaries upon aerodynamic sound," *Proc. R. Soc. Lond. A*, Vol. 231, No. 1187, 1955, pp. 505–514.

[30] Rahier, G., Huet, M., and Prieur, J., "Additional terms for the use of Ffowcs Williams and Hawkings surface integrals in turbulent flows," *Comp. & Fluids*, Vol. 120, 2015, pp. 158–172.

[31] Ikeda, T., Enomoto, S., Yamamoto, K., and Amemiya, K., "Quadrupole Corrections for the Permeable-Surface Ffowcs Williams–Hawkings Equation," *AIAA Journal*, 2017, pp. 2307–2320.

[32] Shur, M. L., Spalart, P. R., and Strelets, M. K., "Noise prediction for increasingly complex jets. Part I: Methods and tests," *International journal of aeroacoustics*, Vol. 4, No. 3, 2005, pp. 213–245.